



Intravital analysis of vascular permeability in mice using two-photon microscopy

Gyohei Egawa, Satoshi Nakamizo, Yohei Natsuaki, Hiromi Doi, Yoshiki Miyachi & Kenji Kabashima

Department of Dermatology, Kyoto University Graduate School of Medicine, Kyoto, Japan.

SUBJECT AREAS:

FLUORESCENCE
IMAGING

BLOOD FLOW

IMMUNOLOGICAL MODELS

TIME-LAPSE IMAGING

Received
5 April 2013

Accepted
1 May 2013

Published
4 June 2013

Correspondence and
requests for materials
should be addressed to
K.K. (kaba@kuhp.
kyoto-u.ac.jp)

Blood vessel endothelium forms a semi-permeable barrier and its permeability controls the traffics of plasma contents. Here we report an intravital evaluation system for vascular permeability in mice using two-photon microscopy. We used various sizes of fluorescein-conjugated dextran as a tracer and its efflux was quantified by measuring the changes of fluorescent intensity both on the blood vessel area and the interstitial space. Using this system, we demonstrated that skin blood vessels limited the passage of dextran larger than 70 kDa under homeostatic conditions. We evaluated the kinetics of vascular permeability in histamine- or IgE-induced type I allergic models and a hapten-induced type IV allergic model. In such inflammatory conditions, the hyperpermeability was selectively induced in the postcapillary venules and dextran as large as 2000-kDa leaked from the bloods. Taken together, our study provides a convenient method to characterize the skin blood vessels as a traffic barrier in physiological conditions.

The vascular system has a variety of functions including supplying nutrients, recruiting immune cells, and maintaining tissue fluid homeostasis. These functions are dependent on the endothelial cells lining the vasculature that provides a semi-permeable barrier between blood contents and the tissue interstitium. Of note, the permeability changes drastically depending on the physiological state of the surrounding tissues and affects the regulation of plasma protein distribution that controls the homeostasis of interstitial fluids¹⁻³.

Understanding the transport of plasma proteins through the vessel wall is a major issue for vascular physiology; however, the assessment of vascular permeability is complicated because it is affected by multiple factors including the type of microvessels, the size and charge of extravasating molecules, and the anatomic pathway that molecules take to traverse the endothelium. Conventionally, the vascular permeability has been evaluated *in vitro* or through the Miles assay using living animals. A number of groups have used an *in-vitro* assay system that measures the flux of variety sizes of molecules that traverse endothelial cells cultured in transwell chambers⁴⁻⁶. These assays are relatively easy to perform, however, it should be noted that the monolayer of endothelial cells in this assay system is generally more leaky because it lacks the pericytes and smooth muscles that surround vascular endothelial cells *in vivo*. Miles assay is another widely used system to measure the vascular permeability^{7,8}. Typically, tracers such as Evan's blue that bind noncovalently to albumin or isotope-labeled albumin are injected intravenously, and the accumulated tracer is later quantified at a test site on the skin. The limitation of the Miles assay is that it is not suitable for the assessment of vascular permeability in non-inflammatory tissue because the tracers used do not traverse the vascular barrier in significant quantities in the absence of inflammation.

In this study, we report an intravital evaluation system for vascular permeability in mice using two-photon microscopy. Two-photon microscopy offers real-time, high-resolution images of endogenous fluorescent molecules in living tissues with little or no tissue damage⁹⁻¹¹. We used various sizes (20–2000 kilodaltons (kDa)) of fluorescein-conjugated dextran and directly monitored and quantified their leakage from the bloods *in vivo*. Using this system, we characterized the size-dependent properties of the vascular barrier both in homeostatic and inflammatory conditions.

Results

Bloodstream visualization and quantification of leakage *in vivo*. To visualize the bloodstream *in vivo*, we used fluorescein isothiocyanate-conjugated dextran (FITC-dextran) as a tracer. Dextran is a polysaccharide that consists of glucose chains and its molecular mass is variable from 3 to 2000 kDa. BALB/c mice were anesthetized and FITC-dextran was injected via the tail vein, while skin on the ventral side of the ear was observed under a two-photon microscope. In this way, arterioles were delineated immediately after dextran

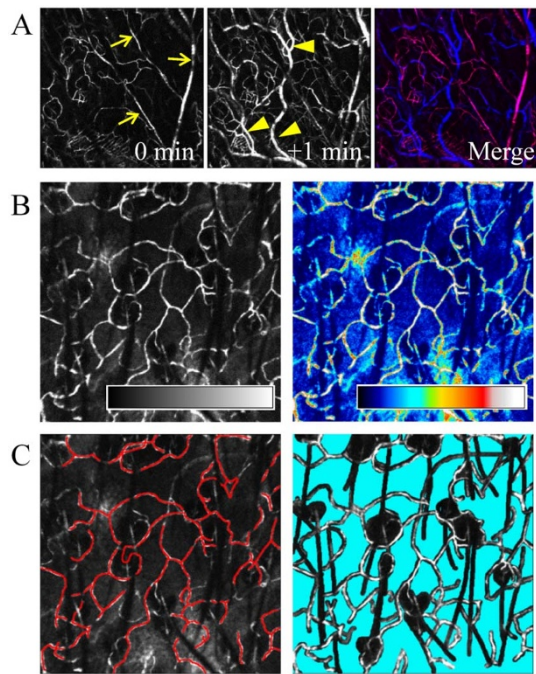


Figure 1 | Bloodstream visualization with fluorescent-dextran. (A) FITC-dextran injection first delineated arterioles (arrows) and then capillaries and postcapillary venules (arrow heads). The merged image depicts vessels at 0 min (red) and 1 min (blue) after the injection, respectively. (B) The black-and-white images (left) were converted to rainbow color-scale images (right) according to fluorescent intensity. (C) The blood vessel area (left: red) and the interstitial space (right: cyan) were separately circumscribed to monitor the fluorescent intensity.

injection and visualization of capillaries and postcapillary venules followed, thus allowing us to distinguish blood vessel types (Fig. 1A). The black-and-white images obtained were then converted to rainbow color-scale images according to fluorescent intensity (Fig. 1B). To monitor tracer dynamics, we separately circumscribed the blood vessel area and interstitial space (Fig. 1C) and quantified the mean fluorescent intensity (MFI) of these areas minute by minute.

Vascular permeability under homeostatic conditions. Using this system, we first evaluated basal vascular permeability under homeostatic conditions (Fig. 2A and supplementary video S1). When we injected 20-kDa FITC-dextran, the tracer readily leaked into the interstitial space and the MFI of the interstitium peaked around 10 min after injection (Fig. 2A, B, and E). In addition, fluorescent signals from the tracer had almost completely disappeared 60 min later (Fig. 2A, B, and F). On the other hand, 40-kDa dextran exhibited mild but sustained leakage, as indicated by a persistent elevation of the MFI in the interstitial space (Fig. 2C, E, and F). As for 70-kDa dextran, most of the tracer was retained within the blood and the MFI of the interstitial space was not elevated at up to 60 min after injection (Fig. 2D–F). Similar dynamics were observed when dextran larger than 70 kDa was injected (Fig. 2E and F). To directly examine the kinetics of plasma proteins, we next used FITC-conjugated bovine albumin as a tracer, whose molecular size is 66-kDa (Fig. 2G). As with 70-kDa dextran, FITC-albumin was retained in the blood 10 min after injection (Fig. 2E); however, a mild elevation of the interstitial space MFI was observed after 60 min (Fig. 2F).

Vascular hyper-permeability under inflammatory conditions. We next evaluated the size-barrier property of skin blood vessels under inflammatory conditions. To mimic vascular hyper-permeability induced by inflammation, we used intravenous injections of histamine and visualized the bloodstream with FITC-dextran. In contrast

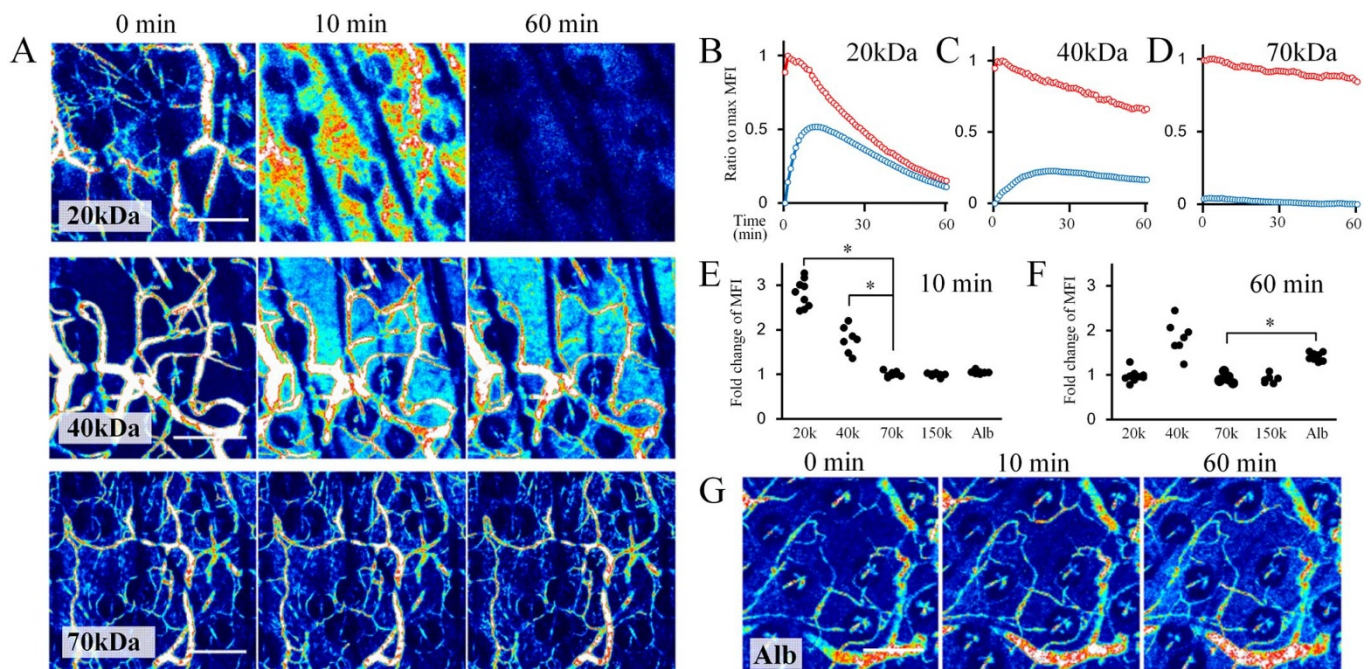


Figure 2 | Vascular permeability under basal conditions. (A) Sequential images taken 0, 10, and 60 min after FITC-dextran injection. The molecular sizes of the injected dextran are shown in the bottom left of each image. (B–D) Kinetics of the MFI in the blood vessel area (red) and interstitial space area (blue) following injection of 20 kDa, 40 kDa, and 70 kDa dextrans, respectively. All experiments were performed at least three times with similar findings. (E, F) Fold change of the MFI in the interstitial space at 10 min or 60 min after the injection of FITC-dextran (20–150 kDa) or albumin. MFI in the interstitial space at 1 min was used as basis. * $P < 0.05$. (G) Sequential images of FITC-albumin injection. Scale bar = 100 μm .

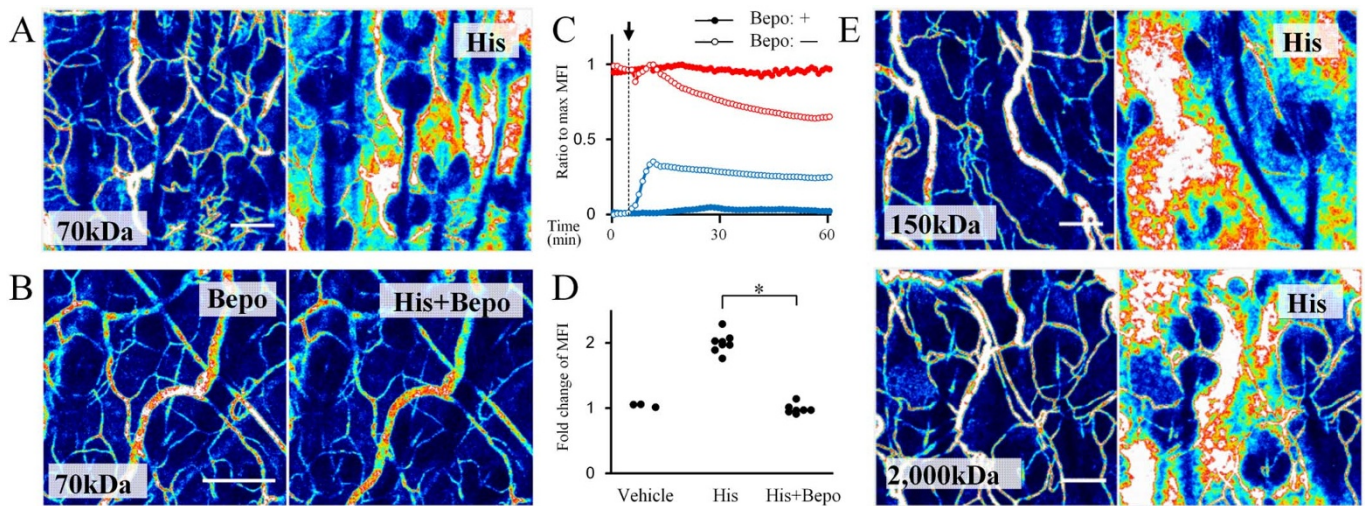


Figure 3 | Vascular hyper-permeability induced by injection of histamine. (A, B) Sequential images before (left) and 5 min after (right) histamine injection. Mice were pretreated with an antihistamine agent, bepotastine besilate or vehicle 1 hour before injection. (C) Kinetics of the MFI in the blood vessel area (red) and in the interstitial space (blue). The arrow denotes the timepoint of histamine injection. Mice were pretreated with bepotastine (closed circles) or vehicle (open circles). (D) Fold changes of the MFI in the interstitial space 5 min after the injection of vehicle or histamine with or without antihistamine pretreatment. MIF at 1 min before the injection was used as basis. $*P < 0.05$. (E) Sequential images before (left) and 5 min after (right) histamine injection. The molecular sizes of the injected dextran are shown in the bottom left of each image. His; histamine, Bepo; bepotastine besilate. Scale bar = 100 μ m.

to homeostatic conditions, 70-kDa dextran shifted into the interstitial space 1–2 mins after the histamine injection (Fig. 3A and supplementary video S2). This leakage of tracer was completely histamine-dependent, since pretreatment with a histamine receptor-1 antagonist, bepotastine besilate, blocked extravasation of the tracer

(Fig. 3B–D). Similarly to 70-kDa dextran, 150-kDa and even 2000-kDa dextran shifted into the interstitial space within 2 mins (Fig. 3E). These observations indicate that inflammation elevates vascular permeability such that plasma contents of up to 2000-kDa can pass through.

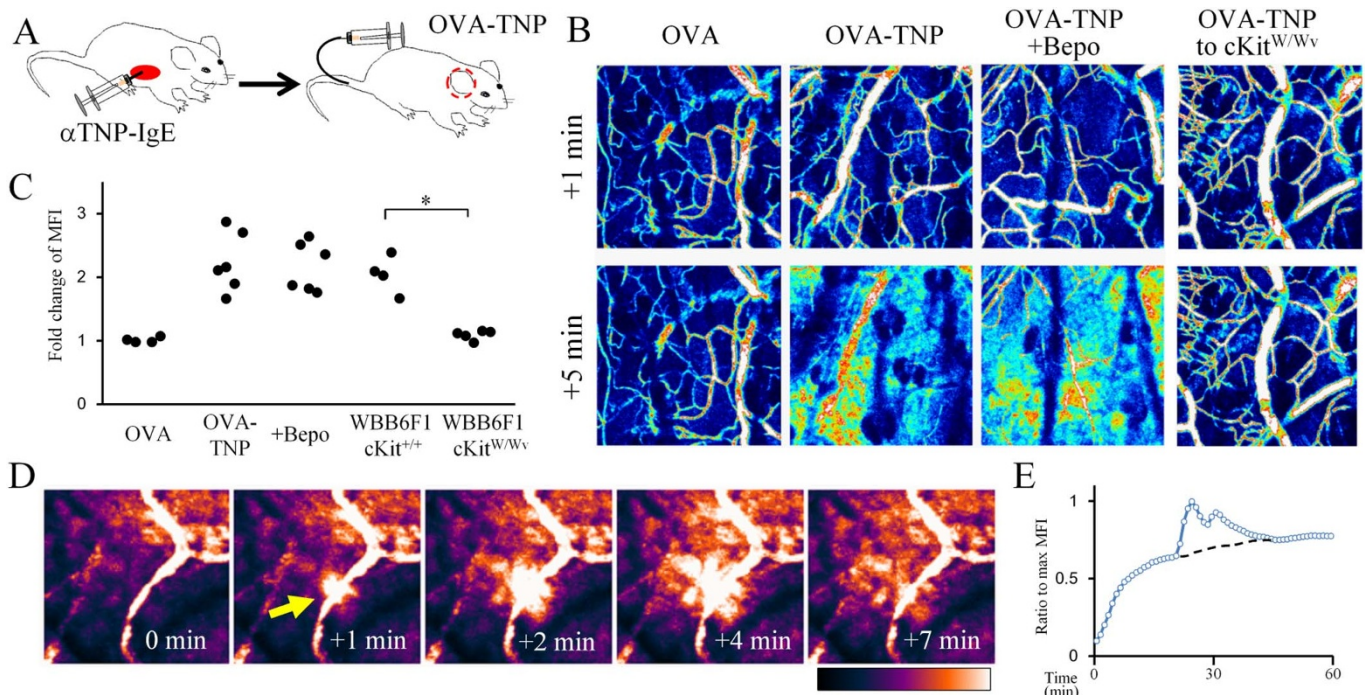


Figure 4 | Vascular hyper-permeability in models of anaphylaxis and CHS. (A) Passive anaphylaxis model. Anti-TNP IgE antibody was injected intraperitoneally into mice. The following day, vascular permeability was analyzed in the ear after an intravenous injection of OVA-TNP. (B) Sequential images 1 and 5 minutes after the injection of OVA and OVA-TNP with or without bepotastine in the passive anaphylaxis model. In the rightmost panel, OVA-TNP was injected into WBB6F1-kit^{W/Wv} mice. (C) Fold change of the MFI in the interstitial area 5 min after the OVA or OVA-TNP injection. MIF at 1 min before the injection was used as basis. $*P < 0.05$. (D) Serial images of the bloodstream in CHS-induced inflamed skin. The arrow indicates transient hyper-permeability in a localized area. Elapsed time is shown in the bottom right of each image. (E) Kinetics of the MFI in the interstitial space in (D). The dotted line represents the predicted baseline in this area.



Visualization of vascular hyper-permeability in classical models of allergy. To examine the change of vascular permeability in more physiological settings, we used the passive anaphylaxis model as a classical type I allergic reaction. IgE antibody against TNP was injected intraperitoneally, followed by intravenous injection of TNP-conjugated OVA (Fig. 4A). The induction of anaphylaxis was clearly visualized with OVA-TNP, while the injection of non-conjugated OVA had no effect on permeability (Fig. 4B). This hyper-permeability was not suppressed with bepotastine besilate treatment but was suppressed in WBB6F1^{W/W^v} mice in which mast cells were absent, suggesting that mast cells but not histamine were indispensable in this model.

We then examined hyper-permeability in a CHS model, as a classical type IV allergic reaction¹². T cells from DNFB-sensitized mice were transferred into non-sensitized mice and DNFB was painted on the ear skin. Twenty hours later, injected dextran readily leaked from postcapillary venules (Supplementary video S3), as shown by histamine injection. Intriguingly, we frequently observed transient leakages of tracer in localized areas (Fig. 4C). Such transient hyper-permeability lasted only about 5 min (Fig. 4D and E), demonstrating that hyper-permeability is strictly regulated and can be resolved within a short time under physiological conditions.

Hyper-permeability occurs in postcapillary venules. As shown in Figure 1, the advantage of our system is to distinguish blood vessel types *in vivo*. This enabled us to examine the location of tracer leakage in real-time. We separately measured the MFI on arterioles, capillaries, and venules (Fig. 5A), and demonstrated that just after the histamine injection, leakages of tracer were detected around postcapillary venules (Fig. 5B; arrows, and supplementary video S2), but not around arterioles or capillaries. In addition, some parts of postcapillary venules became undetectable thereafter (Fig. 5B; arrowheads). Consistent with this, the MFI of postcapillary venules was significantly decreased compared to that of arterioles and capillaries (Fig. 5C). These observations indicate that the permeability is selectively elevated in the postcapillary venules. Since a previous report using a hamster cheek pouch demonstrated that leukotriene-induced hyper-permeability occurred in postcapillary venules¹³ and leukocyte extravasation is observed in this domain¹⁴, it is likely that postcapillary venules play an important role in the induction of inflammation.

Discussion

In this study, we reported an intravital evaluation system for vascular permeability with two-photon microscopy and characterized the basal size-limitation of skin microvessels in mice. The major advantages of this method are as follows; (1) the dynamic kinetics of vascular permeability is determined in real-time, (2) the permeability could be evaluated without introducing inflammations, (3) the types of blood vessels, such as arterioles, venules, and capillaries are readily distinguished. Thus this method should provide a novel convenient way to study vascular biology *in vivo*. Though we examined only the characteristics of skin microvessels, this method may be applicable to examine the vessel permeability in other internal tissues such as in the brain.

Using this system, we demonstrated that dextran larger than 70 kDa was retained in the blood for hours under homeostatic conditions, indicating that a traffic restriction exists for plasma contents around 70-kDa (Fig. 6). This observation is physiologically convincing because not only albumin (molecular weight (MW) = 66 kDa) but also other carrier proteins in plasma, such as transferrin (MW = 80 kDa), transthyretin-tetramer (MW = 56 kDa), and thyroxine-binding globulin (MW = 54 kDa) represents similar molecular sizes (Fig. 6; orange). We also demonstrated FITC-albumin was observed in the interstitial space approximately one hour after administration. Others have shown the specific transport of albumin *in vivo* and *in vitro* via caveolae^{15,16} and, importantly, have even demonstrated the role of caveolae-mediated transport of albumin during inflammation¹⁷. Therefore, visualizing the activation of albumin transport and the role of caveolae specifically in caveolin-1 null mice will be an intriguing future study. Of note, the permeability of plasma contents is determined not just by molecular size but is also affected by shape, charge and hydrophilicity, thus how such physiological characteristics influence permeability should be examined.

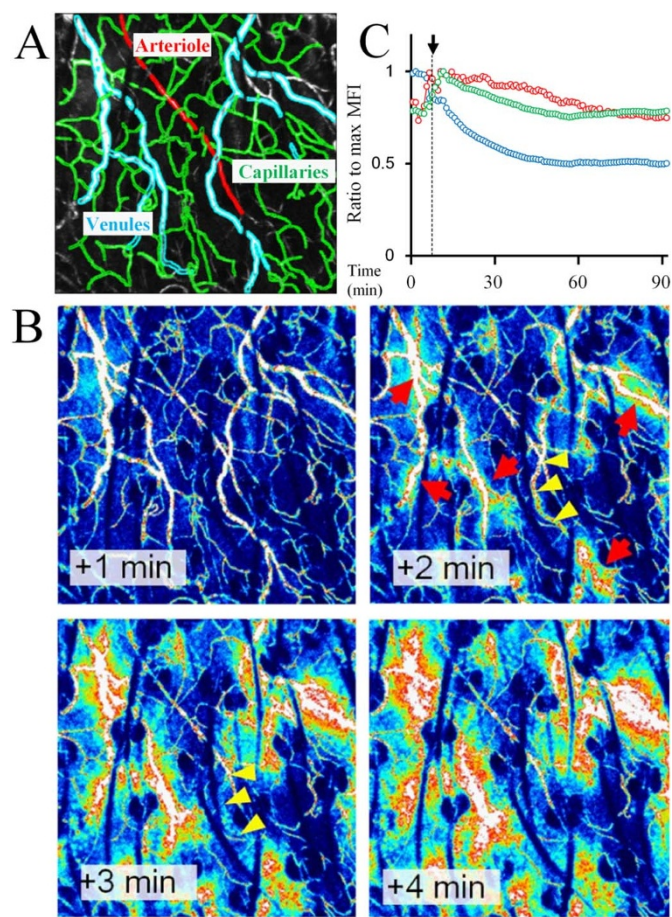


Figure 5 | Hyper-permeability occurs in postcapillary venules. (A) Microvasculature in the ear skin. Arteriole (red), capillaries (green), and post capillary venules (blue) are shown. (B) Sequential images after histamine injection. Elapsed time is shown in the bottom left of each image. Red arrows indicate initiation sites of leakage from postcapillary venules. Some areas of postcapillary venules became undetectable thereafter (yellow arrowheads). (C) Kinetics of the MFI in the area of arterioles (red), capillaries (green), and post capillary venules (blue) after histamine injection. Arrow denotes the timepoint of histamine injection.

Under inflammatory conditions, on the other hand, we observed a dynamic elevation of vascular permeability. Herein, we visualized an elevated vascular permeability in type I and type IV allergy models. Under such conditions, even 2000-kDa dextran promptly shifted into the interstitial space. Since the molecular sizes of immunoglobulins (Igs) range from 146- to 990-kDa (Fig. 6; red), all subclasses of Igs, including IgM, should promptly traverse the vascular endothelium at sites of inflammation. Conversely, the majority of Igs should be basically retained in blood circulation in order to efficiently migrate into sites of inflammation where harmful pathogens have invaded. Extravasation of albumin, a major osmotic protein, results in the expansion of interstitial fluid contributing to wash out of harmful pathogens. Ig is another major plasma protein component mediating humoral immunity. Therefore our study illustrated the other benefit of vascular hyper-permeability in inflammation which,

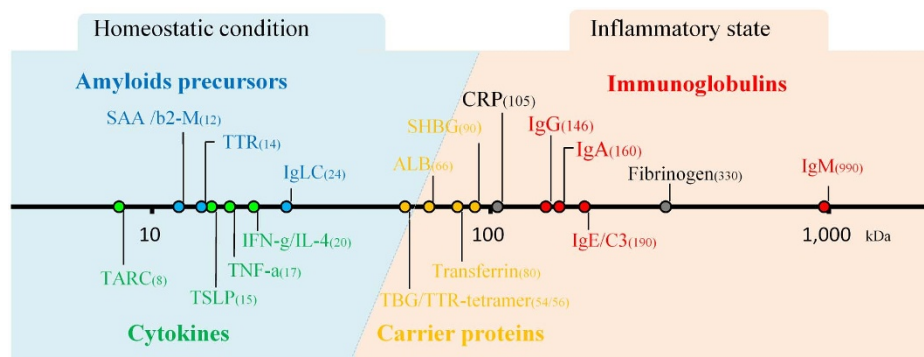


Figure 6 | Molecular size and the permeability of plasma proteins. Molecular size of plasma proteins. TARC: thymus and activation-regulated chemokine; SSA: serum amyloid A; b2-M: b2-microglobulin; TTR: transthyretin; TSLP: thymic stromal lymphopoietin; Ig-LC: immunoglobulin light chain; TBG: thyroxin-binding globulin; ALB: albumin; SHBG: sex hormone binding globulin; CRP: c-reactive protein.

in addition to enabling the wash-out effect, permits the efflux of plasma proteins, particularly immunoglobulins. This should be an essential system that enables selective accumulation of immunoglobulins into sites of inflammation for the clearance of pathogens.

In conclusion, two-photon microscopic system provides a convenient intravital method for analyzing vascular permeability and we propose that understanding vascular permeability as an internal barrier is essential in order to improve our understanding of the pathogenesis of humoral immunity-mediated diseases.

Methods

Mice. Female 8- to 12-week-old BALB/c, WBB6F1^{W/W^v}, and WBB6F1^{+/+} mice were purchased from SLC (Shizuoka, Japan). All experimental procedures were approved by the Institutional Animal Care and Use Committee of Kyoto University Faculty of Medicine.

Time-lapse image acquisition of bloodstream and leakage quantification. Mice were positioned on the heating-plate on the stage of a two-photon microscope, IX-81 (Olympus, Tokyo, Japan) and their ear lobes fixed beneath cover slips with a single drop of immersion oil. To visualize the bloodstream, the tail vein was cannulated using polyethylene tubing (PE-10; Becton, Dickinson and Co, Franklin Lakes, NJ) with a 30-gauge disposable needle (Dentronics, Tokyo, Japan) connected to a syringe filled with a fluorescein tracer; i.e. 5 mg fluorescein isothiocyanate (FITC)-conjugated dextran (20, 70, 150, 2000-kDa; Sigma-Aldrich, St Louis, MO) and 5 mg FITC-albumin (Sigma-Aldrich) dissolved in 500 μ l of phosphate buffered saline (PBS). Stacks of 10 images, spaced 4 μ m apart, were acquired every one minute. The black-and-white images obtained were then converted to rainbow color-scale images according to fluorescent intensity using ImageJ, a free software from National Institutes of Health (NIH). Then the blood vessel area and interstitial space were manually circumscribed and the MFIs of each area were measured minute by minute.

Histamine injection, passive anaphylaxis and contact hypersensitivity (CHS) models.

To induce vascular hyper-permeability, 5 mg histamine (Sigma-Aldrich) dissolved in 500 μ l PBS was injected via tail vein after the bloodstream was visualized using 70 kDa FITC-dextran. To induce antigen-dependent vascular hyper-permeability, mice were injected i.p. with 100 μ g anti- trinitrophenol (TNP) IgE antibody (IGELb4; a kind gift from E. Kuroda), and the following day, 50 μ g ovalbumin (OVA) -TNP (Biosearch Technologies, Novato, CA) were injected via the tail vein. To induce a CHS reaction, mice were sensitized with 25 μ l of 0.5% (w/v) 1-fluoro-2,4-dinitrobenzene (DNFB; Nacalai Tesque, Kyoto, Japan). Six days later, T cells were magnetically sorted from each of the draining lymph nodes and then transferred intravenously into naive mice, and the ear was subsequently challenged with 20 μ l of 0.5% DNFB.

Statistical analysis. The statistical significance of differences between experimental groups was determined with a parametric Student's t-test. P values of less than 0.05 were considered significant.

- Mehta, D. & Malik, A. B. Signaling mechanisms regulating endothelial permeability. *Physiol Rev* **86**, 279–367 (2006).
- Vandenbroucke, E., Mehta, D., Minshall, R. & Malik, A. B. Regulation of endothelial junctional permeability. *Ann N Y Acad Sci* **1123**, 134–145 (2008).
- Nagy, J. A., Benjamin, L., Zeng, H., Dvorak, A. M. & Dvorak, H. F. Vascular permeability, vascular hyperpermeability and angiogenesis. *Angiogenesis* **11**, 109–119 (2008).

- Albelda, S. M., Sampson, P. M., Haselton, F. R., McNiff, J. M., Mueller, S. N. *et al.* Permeability characteristics of cultured endothelial cell monolayers. *J Appl Physiol* **64**, 308–322 (1988).
- Del Vecchio, P. J., Siflinger-Birnboim, A., Shepard, J. M., Bizios, R., Cooper, J. A. *et al.* Endothelial monolayer permeability to macromolecules. *Fed Proc* **46**, 2511–2515 (1987).
- Cooper, J. A., Del Vecchio, P. J., Minnear, F. L., Burhop, K. E., Selig, W. M. *et al.* Measurement of albumin permeability across endothelial monolayers in vitro. *J Appl Physiol* **62**, 1076–1083 (1987).
- Miles, A. A. & Miles, E. M. Vascular reactions to histamine, histamine-liberator and leukotaxine in the skin of guinea-pigs. *J Physiol* **118**, 228–257 (1952).
- Senger, D. R., Galli, S. J., Dvorak, A. M., Perruzzi, C. A., Harvey, V. S. *et al.* Tumor cells secrete a vascular permeability factor that promotes accumulation of ascites fluid. *Science* **219**, 983–985 (1983).
- Cahalan, M. D., Parker, I., Wei, S. H. & Miller, M. J. Two-photon tissue imaging: seeing the immune system in a fresh light. *Nat Rev Immunol* **2**, 872–880 (2002).
- Egawa, G., Honda, T., Tanizaki, H., Doi, H., Miyachi, Y. *et al.* In vivo imaging of T-cell motility in the elicitation phase of contact hypersensitivity using two-photon microscopy. *J Invest Dermatol* **131**, 977–979 (2011).
- Egawa, G. & Kabashima, K. Skin as a peripheral lymphoid organ: revisiting the concept of skin-associated lymphoid tissues. *J Invest Dermatol* **131**, 2178–2185 (2011).
- Honda, T., Egawa, G., Grabbe, S. & Kabashima, K. Update of Immune Events in the Murine Contact Hypersensitivity Model: Toward the Understanding of Allergic Contact Dermatitis. *J Invest Dermatol* (2012).
- Dahlen, S. E., Bjork, J., Hedqvist, P., Arfors, K. E., Hammarstrom, S. *et al.* Leukotrienes promote plasma leakage and leukocyte adhesion in postcapillary venules: in vivo effects with relevance to the acute inflammatory response. *Proc Natl Acad Sci U S A* **78**, 3887–3891 (1981).
- Muller, W. A. Leukocyte-endothelial-cell interactions in leukocyte transmigration and the inflammatory response. *Trends Immunol* **24**, 327–334 (2003).
- Simionescu, M., Gafencu, A. & Antohe, F. Transcytosis of plasma macromolecules in endothelial cells: a cell biological survey. *Microsc Res Tech* **57**, 269–288 (2002).
- Predescu, D. & Palade, G. E. Plasmalemmal vesicles represent the large pore system of continuous microvascular endothelium. *Am J Physiol* **265**, H725–733 (1993).
- Hu, G., Vogel, S. M., Schwartz, D. E., Malik, A. B. & Minshall, R. D. Inter cellular adhesion molecule-1-dependent neutrophil adhesion to endothelial cells induces caveolae-mediated pulmonary vascular hyperpermeability. *Circ Res* **102**, e120–131 (2008).

Acknowledgements

We are grateful to Dr. Masaru Ishii and Dr. Masayuki Amagai for their technical advices. This work was supported in part by Grants-in-Aid for Scientific Research from the Ministry of Education, Culture, Sports, Science and Technology of Japan.

Author contributions

G.E. designed this study and wrote the manuscript. G.E., H.D., S.N. and Y.N. performed the experiments. Y.M. and K.K. directed the project and edited the manuscript.

Additional information

Supplementary information accompanies this paper at <http://www.nature.com/scientificreports>

Competing financial interests: The authors declare no competing financial interests.



License: This work is licensed under a Creative Commons Attribution-NonCommercial-NoDerivs 3.0 Unported License. To view a copy of this license, visit <http://creativecommons.org/licenses/by-nc-nd/3.0/>

How to cite this article: Egawa, G. *et al.* Intravital analysis of vascular permeability in mice using two-photon microscopy. *Sci. Rep.* 3, 1932; DOI:10.1038/srep01932 (2013).